Negative refraction in anisotropic waveguides made from quantum metamaterials

Jonathan R. Plumridge, Robert J. Steed, and Chris C. Phillips
Experimental Solid State Group, Physics Department, Imperial College, Prince Consort Road, London SW7 2AZ, United Kingdom
(Received 15 January 2008; revised manuscript received 21 April 2008; published 22 May 2008)

We describe two metamaterial waveguide designs which display negative refraction. Both use quantum well nanostructures to engineer tunable resonances in the dielectric response, which can be designed using the rules of quantum mechanics. One uses coupling to a "plasmonic" resonance in adjacent metallic layers to enhance the size of the negative refraction effect. The negative refraction appears close to the quantum well intersubband transition energy, and is sensitive to the two-dimensional concentration of electrons within the wells and in adjacent conducting layers, thus offering the potential for switchable devices. These "quantum metamaterials" are highly distributed multilayered optically anisotropic systems with comparatively low absorption in the negatively refracting spectral region, and they can readily be grown by conventional semiconductor epitaxial growth technologies.

DOI: 10.1103/PhysRevB.77.205428 PACS number(s): 78.20.Bh, 78.67.Pt, 73.20.Mf, 73.21.Fg

I. INTRODUCTION

Metamaterials[1] have generated much interest in the field of classical linear optics because of their promise of realizing such exciting concepts as an invisibility cloak[2] or a perfect lens,[3] which hinge on their ability to generate tunable and spatially varying optical properties including negative refraction. In this paper we extend the metamaterial idea by using nanotechnology methods which enable us to engineer materials on a length scale much smaller not just than the wavelength of light, but also the electrons. This gives us a means of controlling the materials' macroscopic electromagnetic response, and hence a route to generating negatively refracting device structures.

Negative refraction and negative index were described theoretically by Veselago[4] in 1968, where he considered two different, but equivalent, physical mechanisms. In essence, the dot product of the Poynting vector and the **k** vector of the traveling wave needs to be negative; this can be achieved either in a material possessing negative group velocity and positive **k** vector (typically by working in the anomalous dispersion region), or in a material with positive group velocity and negative **k** vector (ε and $\mu<0$). Causality implies that both mechanisms will be accompanied by optical absorption,[4] but in practice this can be offset in structures which either provide gain to offset the losses, or which concentrate the fields[5] after the refraction has taken place.

Experimental work on negative refraction typically exploits the anomalous dispersion around the plasma resonance of metallic structures, such as conducting anisotropic slab structures[6] and parallel plate metallic waveguides.[7] In this paper we propose the use of anomalous dispersion around the intersubband transition of a quantum well (QW) to induce negative refraction through the first of the mechanisms described above. We investigate two slab waveguide designs, both based around semiconductor QWs. The first, a "plasmonically coupled" design (Sec. II B) supports a mode similar to the so-called long-range plasmon (LRP) mode[8] familiar from metallic layer studies, and the second (Sec. II C) supports a mode more akin to the transverse magnetic (TM_0) mode of a dielectric slab waveguide.

The effects of varying the two-dimensional (2D) electron density in the quantum wells are modeled, and we show that by increasing the number of electrons in the quantum wells one can induce a negative index region in the dispersion curves of the LRP and TM_0 modes while preserving the ability to efficiently couple plane wave beams directly into the modes without having to use evanescent wave coupling techniques. For device applications, the 2D electron density in the quantum wells could be varied by either optical pumping,[9] or electrical gating.[10]

Section II provides the theoretical framework. In Sec. II A we present a general description of the modes bound to an anisotropic layer but propagating in its plane. Section II B outlines the effective medium approach appropriate for a LRP-type waveguide with quantum wells embedded in it, and Sec. II C details the effective medium approach for a stack of multiple quantum wells (MQWs). In Sec. III we present the dispersion curves, the absorption, the effective refractive index, and the effects of field compression in these two waveguide designs. Section IV is a brief conclusion.

II. THEORETICAL FRAMEWORK

A. Bound modes supported by an anisotropic layer

We start by considering the general case of a central homogeneous slab, of thickness d and anisotropic dielectric tensor $\bar{\varepsilon}_2$. It is clad by a medium of homogeneous and isotropic dielectric constant ε_1 (Fig. 1). ε_1 is real and positive while $\bar{\varepsilon}_2$ is written as

$$\bar{\varepsilon}_2 = \begin{pmatrix} \varepsilon_{xx} & 0 & 0 \\ 0 & \varepsilon_{yy} & 0 \\ 0 & 0 & \varepsilon_{zz} \end{pmatrix}, \tag{1}$$

where $\varepsilon_{xx}=\varepsilon_{yy}$ and ε_{zz} are complex values with as yet no restriction.

We follow the procedures outlined by Yeh[11] and solve Maxwell's equations for the boundary conditions in Fig. 1, to find the linearly polarized modes which are bound in the z direction but which propagate, in the plane of the slab, in the x direction. In the case of the transverse magnetic (TM) po-

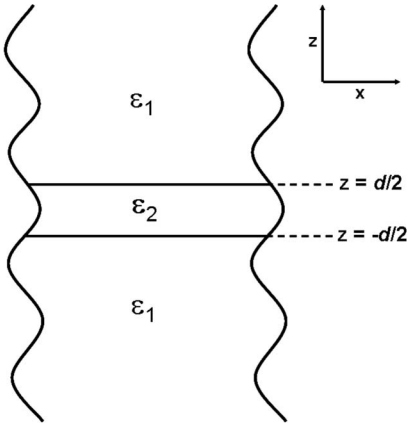

FIG. 1. Schematic of the overall waveguide comprising a central slab, of thickness d, whose anisotropic dielectric response tensor, $\bar{\varepsilon}_2$, is determined by its nanoscale layered structure. It is surrounded by two semi-infinite dielectric layers with the same real, isotropic, and positive dielectric constant, ε_1.

larization, the lowest loss modes are composed of fields at the upper and lower interfaces of the slab, coupled together to give a mode which is symmetrical in z. This mode has dispersion relations given by

$$h \tan(hd/2) = q\varepsilon_{xx}/\varepsilon_1, \tag{2}$$

where h and q are defined by

$$h^2 = K^2\varepsilon_{xx} - k_x^2\varepsilon_{xx}/\varepsilon_{zz}, \tag{3}$$

$$q^2 = k_x^2 - K^2\varepsilon_1, \tag{4}$$

where K is the free-space wave vector. k_x is the x component of the wave vector and is known as the complex propagation constant, $k_x = k_x^{(r)} - ik_x^{(i)}$. The magnetic fields themselves are given by

$$H_y(x,z,t) = \exp[i(\omega t - k_x x)]H_m(z), \tag{5}$$

$$H_m(z) = \begin{cases} A\cos(hz), & |z| < d/2, \\ B\exp(-qz), & z > d/2, \\ B\exp(qz), & z < -d/2. \end{cases} \tag{6}$$

Now, more specifically, we consider a central slab region (with dielectric response $\bar{\varepsilon}_2$) which is made from a multilayered stack of N repeats, each of which is structured at the nanoscale and has a total thickness L_s, giving a central slab thickness $d=NL_s$. L_s is much shorter than the optical wavelength of the mode, allowing us to use an effective medium approach[12] to describe the slab's dielectric response, $\bar{\varepsilon}_2$.

B. Effective medium for "plasmonically coupled" central slab design, using doped metallic layers adjacent to the quantum wells

Figure 2 shows a subunit, of thickness Ls, of such a stack design which features a metallic conducting layer coupled to a closely adjacent quantum well (QW). The metallic layer is a heavily n-doped semiconductor which supports collective

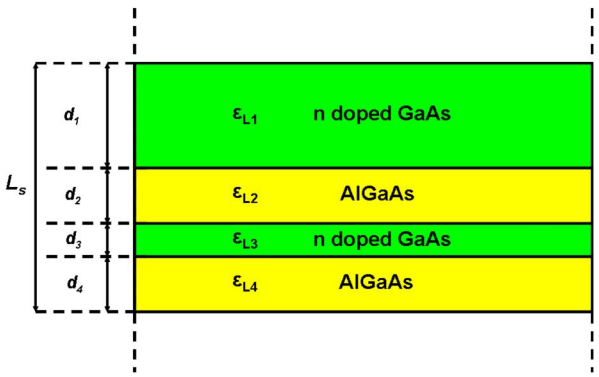

FIG. 2. (Color online) Detail of the layers making a single period of a "plasmonically coupled" quantum metamaterial multilayer which, in turn, makes up the central slab in Fig. 1. Layer 1 acts as a bulk metallic conducting layer whose collective plasma resonance couples electrostatically to the single electron intersubband transitions in the QW, layer 3. The resulting quantum metamaterial behaves as an anisotropic effective medium with the dielectric response tensor $\bar{\varepsilon}_2$ as described in the text.

many-electron plasmonic resonances. It is thin compared to an optical wavelength, but still thick compared to a typical electron wavelength in the semiconductor, so its conductivity can be well approximated by a simple classical Drude model.

The QW on the other hand, as well as being much thinner than an optical wavelength, is also thin enough for the energy spacings of the confined electron states it contains to be larger than kT. Its single particle "intersubband transitions" (ISBT's) have energies, E_{12}, which can be independently tuned, e.g., by the choice of QW design parameters. For the moment we suppose a simple GaAs/AlGaAs single QW design, but more complex multibarrier and coupled QW nanostructure designs can be envisaged for the future. The QW has the extremely anisotropic dielectric response of a 2D electron gas.[13] Fields polarized in the QW plane see a metallic dielectric response but fields polarized normal to the QW layer see an atomiclike response, with a Lorentzian absorption line, centred at E_{12}, whose strength is proportional to the doped-in sheet electron density, n_s.

The Fourier components of the electric field, **E**, generalized displacement, **D**, and electron current density, **j**, are connected by the relation

$$\bar{D}(z,k_x;\omega) = \varepsilon(z)\bar{E}(z,k_x;\omega) + \frac{i4\pi}{\omega}\bar{j}(z,k_x;\omega), \tag{7}$$

where $\varepsilon(z)$ is the background dielectric constant at point z, and k_x is the in-plane component of the photon wave vector. Since we are working in the long wavelength limit, we set $\mathbf{j}(z,k_x;\omega)=\mathbf{j}(z,k_x=0;\omega)$ and omit further references to k_x in the derivation of $\bar{\varepsilon}_2$,

$$\bar{j}(z,\omega) = \bar{E}(z,\omega)\bar{\sigma}(z,\omega). \tag{8}$$

Standard boundary conditions require E_x and D_z to be continuous at the interfaces, but E_z and D_x are discontinuous, and must be suitably averaged over the central slab to obtain its dielectric response when it is viewed as an effective me-

dium. We define the corresponding effective dielectric function as[14]

$$\varepsilon_{xx}(\omega) = \langle D_x(\omega)\rangle / E_x(\omega), \tag{9}$$

$$\varepsilon_{zz}^{-1}(\omega) = \langle E_z(\omega)\rangle / D_z(\omega), \tag{10}$$

where

$$\langle D_x(\omega)\rangle = \frac{1}{L_s}\int_{-L_s/2}^{L_s/2} D_x(z,\omega)dz, \tag{11}$$

$$\langle E_z(\omega)\rangle = \frac{1}{L_s}\int_{-L_s/2}^{L_s/2} E_z(z,\omega)dz. \tag{12}$$

For the four-layer plasmonically coupled design (Fig. 2) Eq. (7) relates the background dielectric constant and current density of each layer to its generalized displacement, $\mathbf{D}(\omega)$. As discussed above, layer 1 is thick enough for its electrons to be treated as a classical 3D Drude gas, and the current distribution in layer 3 is treated as an ideal quasi-two-dimensional sheet. Layers 2 and 4 are undoped and therefore carry no current.

For the quasi-two-dimensional electron gas (layer 3) we have[12]

$$\sigma_{zz}^{(2D)} = \frac{1}{E_z(\omega)}\int_{-\infty}^{\infty} j_z(z,\omega)dz = \frac{j_z^{(2D)}(\omega)}{E_z(\omega)}, \tag{13}$$

which describes the nonretarded response of the electron gas to the z component of the external electric field, $\mathbf{E}$, which we will take to be the z component of the electric field in layer 2. (Later, we will make use of the continuity of D_z across the boundary from layer 2 to layer 3 in the derivation of ε_{zz}.) Assuming for the moment that the QW contains only two strongly confined levels, with only the lower one occupied, using the local density approximation[15] leads to

$$\sigma_{zz}^{(2D)}(\omega) = \Lambda\frac{-i}{[E_{21}^2 - (\hbar\omega)^2]/2\hbar\omega\Gamma - i}, \tag{14}$$

where $\Lambda = n_s e^2 f_{21} h/2m\Gamma$. E_{12} is the intersubband transition energy modified by depolarization effects, $f_{21} = 2mE_{21}(z_{21})^2/h^2$ is the oscillator strength and $\tau = h/\Gamma$ the dephasing time associated with the $1\rightarrow 2$ intersubband transitions. n_s is the sheet electron concentration in the QW, z_{12} the dipole matrix element between the confined states 1 and 2, and e and m are the electron charge and effective mass, respectively.

The parallel conductivity of layer 3 is written as

$$\sigma_{xx}^{(2D)}(\omega) = \frac{1}{E_x(\omega)}\int_{-\infty}^{\infty} j_x(z,\omega)dz = \frac{j_x^{(2D)}(\omega)}{E_x(\omega)}. \tag{15}$$

Again, we assume a Drude-like response and write

$$\sigma_{xx}^{(2D)}(\omega) = \frac{n_s e^2}{m(\tau_\parallel^{-1} - i\omega)}, \tag{16}$$

where $\tau_\parallel (> \tau)$ is the intrasubband relaxation time.

Similarly, for layer 1, also assuming a Drude-like form, we have[16]

$$\sigma_{xx}^{(3D)}(\omega) = \sigma_{zz}^{(3D)}(\omega) = \frac{n_b e^2}{m(\tau_b^{-1} - i\omega)}, \tag{17}$$

where n_b is the bulk 3D electron density and τ_b is the 3D bulk relaxation time.

Using Eqs. (7) and (11)–(17) in Eqs. (9) and (10) yields the following results for the effective medium response for the slab design of Fig. 2. Note that since $L_s \ll \lambda$, then E_x and D_z are practically unchanged over a given period, L_s; $E_x(z,\omega) = E_x(\omega)$ and $D_x(z,\omega) = D_x(\omega)$.

$$\varepsilon_{xx}(\omega) = \tilde{\varepsilon}_x + \frac{i4\pi}{\omega}\tilde{\sigma}_{xx}(\omega), \tag{18}$$

$$\tilde{\varepsilon}_x = \frac{1}{L_s}\sum_i^4 \varepsilon_{Li} d_i, \tag{19}$$

$$\tilde{\sigma}_{xx}(\omega) = \frac{1}{L_s}[\sigma_{xx}^{(3D)}(\omega)d_1 + \sigma_{xx}^{(2D)}(\omega)d_3], \tag{20}$$

and

$$\varepsilon_{zz}^{-1}(\omega) = \tilde{\varepsilon}_z^{-1} - \frac{i4\pi}{\omega}\tilde{\sigma}_{zz}(\omega), \tag{21}$$

$$\tilde{\varepsilon}_z^{-1} = \frac{1}{L_s}\sum_i^4 \varepsilon_{Li}^{-1} d_i, \tag{22}$$

$$\tilde{\sigma}_{zz}(\omega) = \frac{1}{L_s}\left[\frac{\sigma_{zz}^{(3D)}(\omega)d_1}{\varepsilon_{L4}\varepsilon_{L1}} + \frac{\sigma_{zz}^{(2D)}(\omega)d_3}{\varepsilon_{L2}\varepsilon_{L3}}\right], \tag{23}$$

here we have used the continuity of D_z across the boundary of layers 2 and 3 and layers 1–4 in the derivation of Eq. (23).

C. Effective medium description of the doped multiple quantum well (MQW) slab design

Now we consider a simpler design, where the central slab of the structure in Fig. 1 is composed of a doped QW of thickness L_{qw}, surrounded by barrier material making up a period in the multilayer of thickness $L_s = L_{\mathrm{MQW}}$. Our approach is the same as that previously adopted by Zaluzny and Nalewajko[12] and we quote their result:

$$\varepsilon_{xx}^{mqw}(\omega) = \tilde{\varepsilon}_x^{mqw} + \frac{i4\pi}{\omega L_{mqw}}\sigma_{xx}^{(2D)}(\omega)L_{qw}, \tag{24}$$

$$\tilde{\varepsilon}_x^{mqw} = \frac{\varepsilon_b(L_{mqw} - L_{qw})}{L_{mqw}} + \frac{\varepsilon_w L_{qw}}{L_{mqw}}, \tag{25}$$

and

$$\frac{1}{\varepsilon_{zz}^{mqw}(\omega)} = \frac{1}{\tilde{\varepsilon}_z^{mqw}} - \frac{i4\pi}{\omega L_{mqw}\varepsilon_b\varepsilon_w}\sigma_{zz}^{(2D)}(\omega)L_{qw}, \tag{26}$$

$$\frac{1}{\tilde{\varepsilon}_z^{mqw}} = \frac{L_{mqw} - L_{qw}}{\varepsilon_b L_{mqw}} + \frac{L_{qw}}{\varepsilon_w L_{mqw}}. \tag{27}$$

Note the similarities between this result and that obtained in Sec. II B.

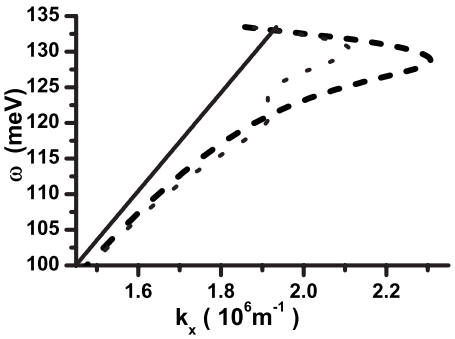

FIG. 3. Dispersion curves for modes propagating in the plane of the plasmonically coupled quantum metamaterial waveguide. Dotted line, case (i) with the QWs doped to a sheet electron density, $n_s=5\times10^{12}$ cm^{-2}. Dashed line, case (ii), with the QWs undoped, $n_s=0$. The intersubband transition in the QW induces a region of negative group velocity at energies around 121 meV/1.84 $\times10^{14}$ s^{-1}. Solid line, light line in vacuum.

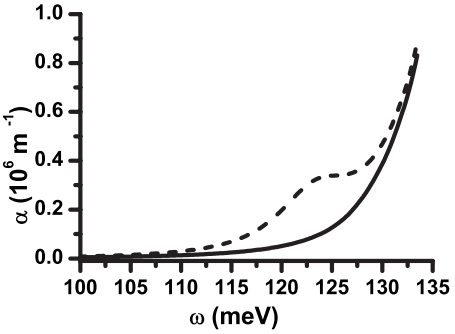

FIG. 4. Absorption coefficient, ω, for radiation traveling in the plane of the plasmonically coupled MQW quantum metamaterial waveguide ($\alpha=2k_x^{(i)}$). Sheet electron density in quantum wells, $n_s=5\times10^{12}$ cm^{-2} (dashed line) and $n_s=0$ (solid line).

III. RESULTS AND DISCUSSION

A. Propagation, absorption, and negative refraction of the plasmonically coupled QW waveguide design

Here we numerically solve Eq. (2) For a structure with a central slab comprising two periods of the plasmonically coupled design in Fig. 2, symmetrically clad with thick cladding layers (Fig. 1). The results allow us to determine the propagation constant, the absorption coefficient, the group velocity, and the effective refractive index. We also compute a figure of merit, $F\equiv k_x^{(r)}/k_x^{(i)}$, the ratio of the real to the imaginary parts of the in-plane propagation constant, as a standard measure of how useful the negative refraction effect will be in a real device structure, when absorption losses have to be accommodated.

We consider two cases; in both the electron concentration in the doped metallic layers is high enough to sustain a long-range plasmon mode,[8] but in case (i) the QWs are heavily doped and in (ii) they are undoped.

The materials parameters (alloy concentrations in brackets) used in the model are as follows: $\varepsilon_{cladding}=8.2067$ ($Al_{0.9}Ga_{0.1}As$), $\varepsilon_{L1}=\varepsilon_{L3}=10.364$ (GaAs), $\varepsilon_{L2}=\varepsilon_{L4}=9.6449$ ($Al_{0.3}Ga_{0.7}As$), $m=0.0665m_e$. We assume a QW designed to have $E_{21}=124$ meV, which, from separate quantum mechanical modeling, corresponds to a dipole matrix element $z_{12}=2.117$ nm. We use an electron scattering time, τ, deduced from typical measured intersubband transition (ISBT) linewidths of $h\Gamma=5$ meV, and we set $\tau_b=\tau_\parallel=\tau$.

In the specific examples considered, the metallic layers are doped to $n_b=10^{19}$ cm^{-3}, the layer thicknesses are $d_1=72$ nm, $d_2=d_4=10$ nm, and $d_3=8$ nm. In case (i) the QWs are doped to $n_s=5\times10^{12}$ cm^{-2} while in case (ii) $n_s=0$.

Figure 3 shows the modeled dispersion relation for this quantum metamaterial, with and without doping in the QWs. The undoped case (ii) yields the well known dispersion curve of a long-range plasmon mode[8] (LRP), and the doped case (i) shows the effects of our anisotropic metamaterial, where the ISBT resonance produces a pronounced kink in the dispersion curve, in the spectral region of the intersubband energy, $E_{12}=124$ meV, of the quantum well.

It is clear, from the dispersion curves in Fig. 3, that the group velocity, $v_g\equiv\partial\omega/\partial k_x$ takes positive and negative values. For the undoped QW case, the onset of negative group velocity occurs around the structures' bulk plasma frequency and corresponds to the long-range plasmon mode—negative refraction from such a layered structure has recently been experimentally verified,[6] and is similar to that seen in a parallel plate metallic waveguide[7] devices.

However, the purpose of this paper is to draw attention to the extra functionality in the negative group velocity induced by the QWs intersubband resonance. This is seen in Fig. 3 where the two curves, corresponding to doped and undoped QWs, respectively, cross at $\omega_l=1.84\times10^{14}$ s^{-1}/121.3 meV, i.e. just below the ISBT energy, E_{12}. Switching the QW electron density, between the values corresponding to the two curves, flips the slope of the dispersion curves and hence the sign of the group velocity at this energy.

At this energy the $1/e$ absorption strength of the mode is 2.59×10^5 m^{-1} in the doped QW case and 6.44×10^4 m^{-1} in the undoped QW case (Fig. 4). These correspond to figure of merit values F=14.8 and 59.8, i.e., considerably larger than the of order unity values commonly seen in negatively refracting devices made from metal-dielectric composites.[6]

B. Propagation, absorption, and negative refraction in a MQW-based quantum metamaterial waveguide

The same concept, i.e., using the tunable anomalous dispersion associated with an ISBT to produce negative refraction, can be extended to a the more familiar case of the TM_0 mode of a symmetrically clad dielectric slab. Previously we considered how such a symmetrical TM_0 MQW slab mode can be strongly coupled to the ISBTs of that MQW.[17] Here we extend the analysis to show that the same coupling mechanism can be used to create a region of negative group velocity with technologically attractive characteristics.

We use the effective medium expressions of Ref. 17 and derive an anisotropic dielectric tensor, $\bar{\varepsilon}_2$, for the central slab of Fig. 1, comprising an MQW stack, symmetrically surrounded by $Al_{0.9}Ga_{0.1}As$ dielectric cladding, with isotropic dielectric constant $\varepsilon_1=8.2067$.

The central slab now consists of $N=70$ repeats of QW, each with $L_{qw}=8$ nm, $L_{mqw}=20$ nm, $E_{21}=124$ meV, $h\Gamma$

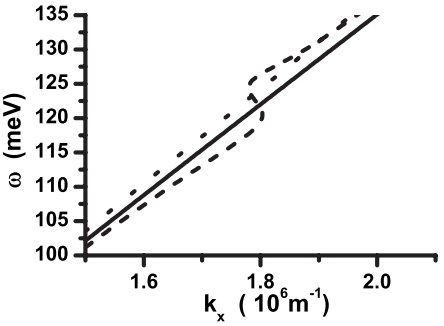

FIG. 5. Dispersion curves for modes propagating in the plane of the MQW waveguide. Dashed line, QWs doped at a sheet electron density, $n_s=4\times10^{11}$ cm^{-2}. Solid line, undoped QWs, $n_s=0$. The ISBT induces a region of negative group velocity around $\omega=1.84\times10^{14}$ s^{-1}/121 meV. Note that, because the "kink" (at $\omega\sim125$ meV) in the dispersion curve of the doped sample lies to the left of the (dotted) light line of the cladding material, these modes can be coupled into directly with incident plane-wave beams.

=5 meV, and $z_{21}=2.117$ nm. To highlight the role of the ISBT we again model two cases, corresponding to the QWs being either undoped or doped at $n_s=4\times10^{11}$ cm^{-2}. The resulting dispersion curves (Fig. 5) show a pronounced region of negative group velocity in the doped samples which, again, flips sign when the electron density is reduced to zero. In the spectral region of interest, $\omega_l=1.85\times10^{14}$ s^{-1}/E_l =121.9 meV, the model yields a $1/e$ absorption length of 2.45×10^5 m^{-1} in the doped sample (Fig. 6), corresponding to a figure of merit F=14.7.

It is important to note that, in the spectral region near ~125 meV, the dispersion curve in Fig. 5, for $n_s=4\times10^{11}$ cm^{-2}, actually crosses over to the left-hand side of the light line for plane waves in the cladding layers. At these frequencies the slab modes' in-plane wave vectors are actually *lower* than those of incident plane-wave beams, so that free space radiation can be efficiently coupled into and out of the slab mode simply by shining in a plane-wave beam at the appropriate angle. This has major practical and technological advantages over other schemes which require contacted prisms or diffraction-grating couplers to couple into the modes of interest.[7]

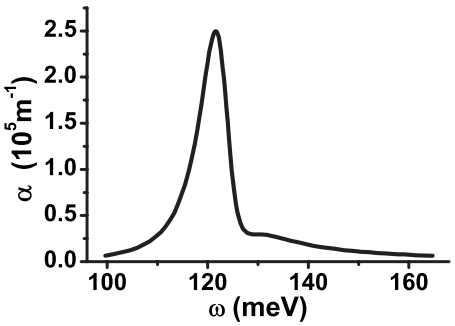

FIG. 6. Absorption coefficient of the MQW waveguide ($\alpha=2k_x^{(i)}$). Sheet electron density, $n_s=4\times10^{11}$ cm^{-2}.

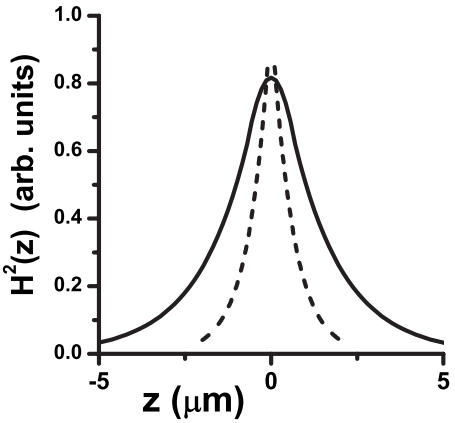

FIG. 7. Mode profiles of the H^2 field for the LRP-like mode of the plasmonially coupled quantum metamaterial waveguide (dashed line) and TM_0–like mode of the MQW dielectric slab waveguide (solid line). The QWs are undoped in ($n_s=0$) in both cases, and ω =121 meV. In the plasmonically coupled sample the fields in the LRP mode are laterally compressed by a factor of ~2.6 over the TM_0 type modes supported by the undoped MQW slab waveguide.

C. Negative refraction and effective negative refractive index

The ideas of group and phase velocity can be used to define an effective refractive index for light propagating in the mode,[7]

$$n_{mode}=\mathrm{sgn}(\bar{v}_p\cdot\bar{v}_g)c/|\bar{v}_p|, \tag{28}$$

In the case of the plasmonically coupled waveguide design (Fig. 3), at the peak ($\omega\sim121$ meV) of the negative refraction effect, "removing" doped-in electrons from the QWs in the model makes this quantity flip sign, from $n_{mode}=3.146$ to −3.121. A similar effect, flipping from n_{mode} 2.918 to −2.904 happens when the electrons are removed from the doped MQW waveguide design (Fig. 5).

In devices analogous to the prism-shaped pieces of metal-metal waveguides of Ref. 7, this sign change could be used to produce rapid and dramatic changes in the angle of refraction in quantum metamaterial waveguide. In principle this effect could be optically switched, either by interband optical pumping,[9] electrical gating,[10] or by designing a three level quantum well with levels 2 and 3 providing the region of negative refractive index (level 2 being optically pumped from level 1).

D. Field enhancement and compression

As can be seen by comparing Figs. 3 and 5, in the case of undoped QWs, the mode dispersion curve moves much further to the right of the cladding light line in the plasmonically coupled sample than it does in the undoped MQW dielectric slab sample, reflecting the increased potential for subwavelength field compression in the former. Figure 7 shows this directly, where the modeled fields of the bare LRP and TM_0 modes show a plasmonic field enhancement effect of ~2.6 at $\omega=121$ meV for comparison ($n_s=0$ in both cases).

IV. CONCLUDING REMARKS

In conclusion, we have proposed two quantum metamaterial waveguides that use the ISBT of incorporated quantum wells to induce a region of negative group velocity, which, in turn, can be used to induce negative refraction effects in a range of device geometries. The effect is strongly dependent upon the 2D electron density in the quantum well, and as such one should be able to pump electrons into the wells (optically or electrically) and thereby make the waveguide into an active component.

The predicted losses in the negative index waveguides, as evidenced by the high figure of merit values, are considerably smaller than typical metal-dielectric schemes, and they all use well established and high quality growth technologies. Also, more complicated quantum well structures could be used to induce gain (or even gain without population inversion[18]) into the medium, thereby overcoming the losses.

ACKNOWLEDGMENT

Funding from the UK Engineering and Physical Sciences Research Council is gratefully acknowledged.

[1] D. R. Smith, J. B. Pendry, and M. C. K. Wiltshire, Science **305**, 788 (2004).
[2] D. Schurig, J. J. Mock, B. J. Justice, S. A. Cummer, J. B. Pendry, A. F. Starr, and D. R. Smith, Science **314**, 977 (2006).
[3] J. B. Pendry, Phys. Rev. Lett. **85**, 3966 (2000).
[4] V. G. Veselago, Sov. Phys. Usp. **10**, 509 (1968).
[5] A. A. Govyadinov and V. A. Podolskiy, Phys. Rev. B **73**, 155108 (2006).
[6] A. J. Hoffman, L. Alekseyev, S. S. Howard, K. J. Franz, D. Wasserman, V. A. Podolskiy, E. E. Narimanov, D. L. Sivco, and C. Gmachl, Nat. Mater. **6**, 946 (2007).
[7] H. J. Lezec, J. A. Dionne, and H. A. Atwater, Science **316**, 430 (2007).
[8] F. Yang, J. R. Sambles, and G. W. Bradberry, Phys. Rev. B **44**, 5855 (1991).
[9] M. Olszakier, E. Ehrenfreund, E. Cohen, J. Bajaj, and G. J. Sullivan, Phys. Rev. Lett. **62**, 2997 (1989).
[10] A. A. Anappara, A. Tredicucci, G. Biasiol, and L. Sorba, Appl. Phys. Lett. **87**, 051105 (2005).
[11] P. Yeh, *Optical Waves in Layered Media* (Wiley, New York, 1988).
[12] M. Zaluzny and C. Nalewajko, Phys. Rev. B **59**, 13043 (1999).
[13] L. Wendler and E. Kandler, Phys. Status Solidi B **177**, 9 (1993); L. Wendler and T. Kraft, Phys. Rev. B **60**, 16603 (1999).
[14] V. M. Agronovich and V. E. Kravtsov, Solid State Commun. **55**, 85 (1985).
[15] T. Ando, Z. Phys. B **24**, 219 (1976).
[16] H. Haug and S. W. Koch, *Quantum Theory of the Optical and Electronic Properties of Semiconductors* (World Scientific, Singapore, 2004).
[17] J. Plumridge and C. Phillips, Phys. Rev. B **76**, 075326 (2007).
[18] M. D. Frogley, J. F. Dynes, M. Beck, J. Faist, and C. C. Phillips, Nat. Mater. **5**, 175 (2006).